View metadata, citation and similar papers at core.ac.uk

brought to you by CORE

provided by Elsevier - Publisher Connector

Available online at www.sciencedirect.com

ScienceDirect

Procedia Engineering 116 (2015) 535 – 543

Procedia Engineering

www.elsevier.com/locate/procedia

8th International Conference on Asian and Pacific Coasts (APAC 2015)

Numerical Simulation of Tsunami Run-up and Inundation Employing Horizontal Two-Dimensional Model Based on CIP Method

Koji Kawasaki[a] * and Kazuki Suzuki[b]

[a]*Hydro-soft Technology Institute, Co., Ltd. Nakanoshima Daibiru 26F, 3-3-23, Nakanoshima, Kita-ku, Osaka 530-6126, Japan*
[b]*Kajima Corporation, 1-3-1, Motoakasaka, Minato-ku, Tokyo 107-8388, Japan*

Abstract

A two-dimensional tsunami run-up and inundation model based on a CIP method was developed in this study so as to satisfy the continuity equation with reasonable accuracy. Numerical simulations on tsunami bore were carried out in order to validate the model and discuss the effects of wet-dry condition and overflow condition on the calculation accuracy. As a result, the model was confirmed to be able to represent closely actual water surface profile by using the slip condition on the wet-dry condition. Furthermore, the numerical results without the overflow formula were found to be in good agreement with the experimental ones.

© 2015 The Authors. Published by Elsevier Ltd. This is an open access article under the CC BY-NC-ND license (http://creativecommons.org/licenses/by-nc-nd/4.0/).

Peer- Review under responsibility of organizing committee , IIT Madras , and International Steering Committee of APAC 2015

Keywords : CIP method; run-up simulation; wet-dry condition; overflow condition; tsunami bore

1. Introduction

Tsunami damages in coastal zones have occurred even in recent years. Advance provision of useful information such as hazard maps and evacuation routes to the peripheral people is considered to be necessary in order to prevent and minimize the damage. Thus, development of an accurate depth-averaged inundation flow numerical model,

* Corresponding author. Tel.: +81-6-6479-3621; fax: +81-6-6479-3622.
E-mail address: kawasaki@hydro-soft.co.jp

1877-7058 © 2015 The Authors. Published by Elsevier Ltd. This is an open access article under the CC BY-NC-ND license (http://creativecommons.org/licenses/by-nc-nd/4.0/).

Peer- Review under responsibility of organizing committee , IIT Madras , and International Steering Committee of APAC 2015
doi:10.1016/j.proeng.2015.08.323

which is suitable for large scale inundation simulations, is required to predict tsunami inundation areas precisely and efficiently.

Inundation simulations have been, in general, conducted using depth-averaged inundation models based on shallow water equations. In recent decades, the various models have been developed for simulate coastal inundation, which can be categorized according to numerical methods to solve the equations: the finite difference method (FDM), the finite element method (FEM) and the finite volume method (FVM). Recently, there have been many studies about numerical schemes in the finite volume method (e.g. Yoon and Kang,2004; Liang and Marche, 2009). Liang and Marche (2009) proposed a well-balanced numerical scheme for simulating depth-averaged inundation flow. However, there have been few studies in terms of the effects of wet-dry condition and overflow condition on the calculation accuracy although the treatments of an overflow process over seawalls and a wet-dry boundary are important for depth-averaged flood inundation simulations.

Based on the above-mentioned, the purpose of the present study is to develop a depth-averaged flood inundation flow model in the Cartesian coordinate system using a CIP (Constrained Interpolation Profile) method, which is able to solve the advection equation precisely taking advantage of the hyperbolic equation. Furthermore, numerical simulations on tsunami bore are performed to validate the model and discuss the effects of the wet-dry condition and the overflow condition on the calculation accuracy.

2. Depth-averaged flood inundation flow model

2.1. Governing equations

The governing equations are shallow water equations in the Cartesian coordinate system, which consist of the continuity equation (Eq. (1)) and the momentum equations (Eqs. (2) and (3)) in the respective directions of x and y on a horizontal plane.

Continuity equation:

$$\frac{\partial H}{\partial t}+\frac{\partial (UH)}{\partial x}+\frac{\partial (VH)}{\partial y}=0 \tag{1}$$

Momentum equations:

$$\frac{\partial (UH)}{\partial t}+\frac{\partial}{\partial x}(U^2H)+\frac{\partial}{\partial y}(UVH)=-gH\frac{\partial (H+z_b)}{\partial x}-\frac{gn^2U}{H^{1/3}}\sqrt{U^2+V^2} \tag{2}$$

$$\frac{\partial (VH)}{\partial t}+\frac{\partial}{\partial x}(UVH)+\frac{\partial}{\partial y}(V^2H)=-gH\frac{\partial (H+z_b)}{\partial y}-\frac{gn^2V}{H^{1/3}}\sqrt{U^2+V^2} \tag{3}$$

where H is the water depth, U and V are the depth-averaged velocities in the x- and y-directions, g is the gravity acceleration, z_b is the ground elevation, and n is Manning's roughness coefficient. The discharge per unit width in the x- and y-directions can be expressed as a product of the total water depth and depth-averaged velocity, as shown in Eqs (4) and (5).

$$q_x = UH \tag{4}$$

$$q_y = VH \tag{5}$$

2.2. Computational algorithm

The governing equations (2) and (3) are separated into an advection step (Eqs. (6) and (7)) and a non-advection step (Eqs. (8) and (9)) using a time splitting method. The resultant equations were discretized by using staggered grids. A CIP method with third-order accuracy, which is developed by Yabe and Aoki (1991), is employed to calculate the hyperbolic equations for depth-averaged velocities U and V at the advection step. The CIP method has been widely used in computational fluid dynamics (eg. Yabe et al., 2001; Kawasaki, 2005), which can provide accurate and less dissipative solutions for the hyperbolic equations. On the other hands, the equations at the non-advection step are solved by using a simultaneous iteration method for velocity and water depth to satisfy the continuity equation with reasonable accuracy.

Advection step:

$$\frac{\partial U}{\partial t}+U\frac{\partial U}{\partial x}+V\frac{\partial U}{\partial y}=0 \tag{6}$$

$$\frac{\partial V}{\partial t}+U\frac{\partial V}{\partial x}+V\frac{\partial V}{\partial y}=0 \tag{7}$$

Non-Advection step:

$$\frac{\partial U}{\partial t}=-gH\frac{\partial (H+z_b)}{\partial x}-\frac{gn^2U}{H^{1/3}}\sqrt{U^2+V^2} \tag{8}$$

$$\frac{\partial V}{\partial t}=-gH\frac{\partial (H+z_b)}{\partial y}-\frac{gn^2V}{H^{1/3}}\sqrt{U^2+V^2} \tag{9}$$

3. Numerical simulations of tsunami run-up and inundation

The model developed here was applied to hydraulic model experiments on tsunami run-up and inundation over a seawall (Arimitsu et al., 2012) in order to validate the model and discuss the effects of wet-dry condition and overflow condition on the calculation accuracy.

3.1. Numerical condition

Computational conditions are shown in Table 1. In this study, numerical simulations were conducted under varying wet-dry condition and overflow condition, the details of which are described in the following subsection. Figure 2 illustrates a schematic of the computational domain. The origin of x axis locates at the edge of the land, and the positive direction was set toward the right hand side of the computational domain. In order to fit the experimental condition, a Manning coefficient n was set to be 0.005 $m^{-1/3}s$ based on preliminary simulations. A wall boundary was imposed at the upstream boundary, and an open boundary condition was set at the downstream. The non-slip condition was selected for the side walls.

3.2. Wet-dry condition

Wet-dry condition is required for treating wave front in tsunami run up and inundation simulation. In this study, two different conditions were considered as the wet-dry condition: the zero-velocity condition based on Kotani et al. (2009) and the slip condition proposed by Kawasaki et al. (2004).

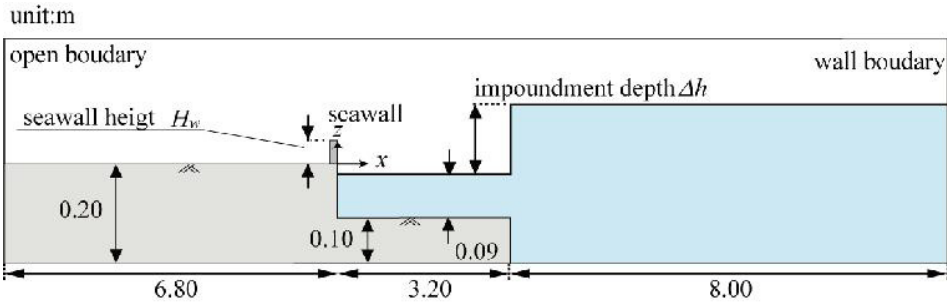

Figure 1. Computational domain.

Table 1. Computational conditions.

Horizontal grid size Δx [m]	0.01
Time interval Δt [s]	0.0005
Manning coefficient n [$m^{-1/2}s$]	0.005
Impoundment depth Δh [m]	0.18
Seawall height H_w [m]	0.00(absence of a seawall), 0.02, 0.05, 0.07, 0.09, 0.11
Threshold depth H_s [m]	0.001
Wet-dry condition	zero-velocity condition, slip condition
Overflow condition	with overflow formula, without overflow formula

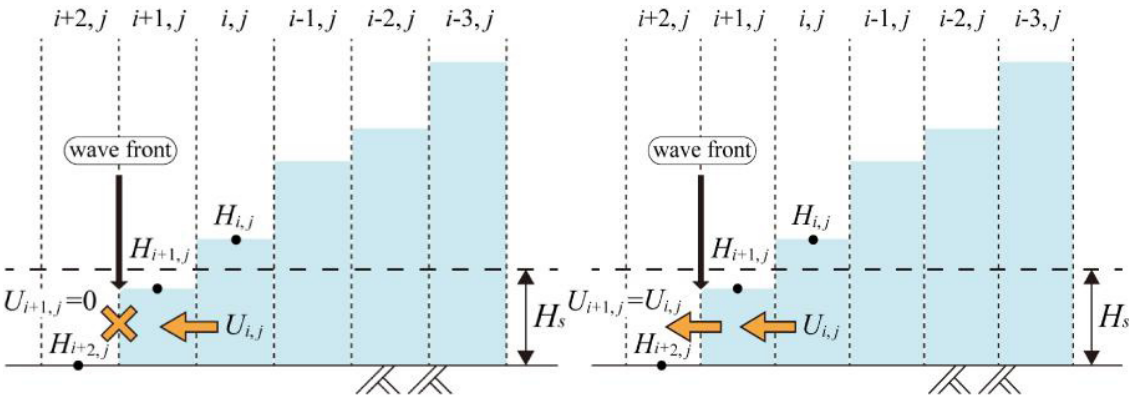

(a) Zero-velocity condition based on Kawasaki et al. (2004) (b) Slip condition based on Kawasaki et al. (2004)

Figure 2. Schematics of wet-dry conditions.

Figure 2 (a) shows the schematics of the zero-velocity condition. If the water depth H is less than the threshold depth H_s, the grid is regarded as dry. In the figure, when the total depth $H_{i,j}$ at the grid point (i, j) is greater than the threshold depth H_s and $H_{i+1,j}$ at the grid point $(i+1, j)$ is less than H_s, the wave front is defined between the grid points (i, j) and $(i+1, j)$ and the depth-averaged velocity $U_{i+1,j}$ at the front is set to zero. In a non-advection step, bottom friction term in Eqs. (8) and (9) are neglected when the water depth $H_{i,j}$ is less than H_s to avoid computational divergence.

The slip condition proposed by Kawasaki et al. (2004) is almost similar to the zero-velocity condition except that a zero velocity gradient condition is imposed at a wave front boundary. The depth-averaged velocity $U_{i+1,j}$ at the wave front is set to equal the $U_{i,j}$ at the (i, j), as shown in Fig. 2 (b).

3.3. Overflow condition

The flow discharge over seawalls, breakwaters and coastal dykes has often been evaluated by the Honma formula (Eqs. (10) and (11); Honma, 1940) in conventional tsunami run-up and inundation simulations. In the present study, the numerical simulation under two different overflow conditions (with and without the overflow formula) were performed in the cases with the seawall. The seawall was incorporated as the topography in the computational domain, and the discharge was calculated by the momentum equations (Eqs. (2) and (3)).

Complete and incomplete overflows:

$$q = 0.35h_1\sqrt{2gh_1} \qquad h_2 \le 2/3h_1 \tag{10}$$

Submerged overflow:

$$q = 0.91h_2\sqrt{2g(h_1 - h_2)} \qquad h_2 > 2/3h_1 \tag{11}$$

where q is the overflow discharge, and h_1 and h_2 are the water depths from the top of the seawall at the front and back of the seawall, respectively.

4. Numerical Results and discussion

4.1. Effect of wet-dry condition

Figure 3 shows the time variations of the water surface profile and the horizontal velocity distribution in the case of the seawall height H_w = 0.00 m (absence of a seawall), in which (a) and (b) indicate the numerical results using

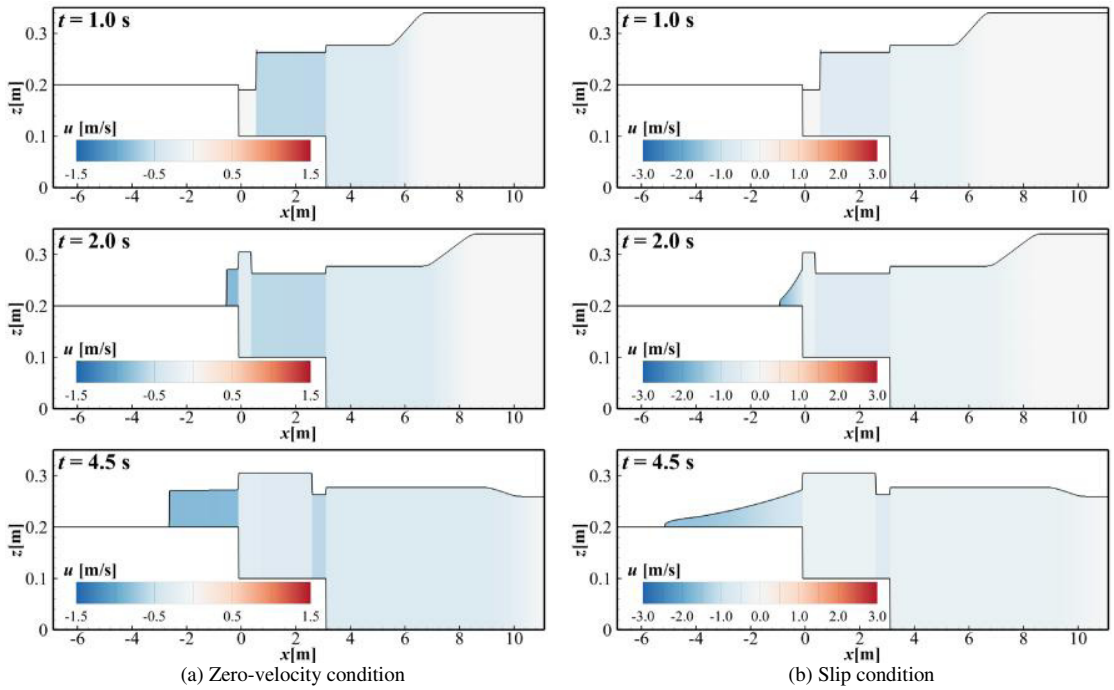

(a) Zero-velocity condition (b) Slip condition

Figure 3. Time variations of water surface profile and horizontal velocity distributions in the case of H_w = 0.00 m (absence of a seawall).

the zero-velocity and the slip condition, respectively. Note that the overflow condition was not used in these cases. The time $t = 0$ was defined as the time when a bore reached at 2 meters off the seawall ($x = 2.0$ m) in this study. Just after the initiation of the simulation, the water column causes a bore, which propagates to the left side. A bore run-up takes place and a reflected wave is generated at the edge of the land at $t = 2.0$ s. It can be also seen from Fig. 3 that the water surface profile near the wave front are different between the slip and zero-velocity conditions after the bore run-up ($t > 2.0$ s). In the case of the zero-velocity condition shown in Fig. 3 (a), the wave front rises steeply while the smooth surface profile is observed near the wave front in the case of the slip condition shown in Fig. 3 (b)

The time variations of the inundation depth and the horizontal velocity at $x = -1.0$ are shown in Figs. 4 (a) and (b), in which red and blue lines show the numerical results using the zero-velocity and the slip conditions, respectively, and black circles show the experimental results. There is a difference in terms of the rising time of the inundation depth and the horizontal velocity between the two cases, and the arrival time for the zero-velocity condition is found to be faster than that for the slip condition. In the zero-velocity condition, the inundation depth rises steeply right after the bore passed, and the inundation depth continues approximately constantly until t= about 10 s, which is different to that observed in the laboratory experiments. On the other hand, the numerical result obtained by using the slip condition reproduces the experiment ones with high accuracy. Thus, the model developed here is found to be capable of representing closely actual water surface profile by using the slip condition on the wet-dry condition.

As for the time series of the horizontal velocity shown in Fig. 4 (b), the numerical result with the zero-velocity condition underestimates the experimental one whereas a good agreement is obtained between the numerical result with the slip condition and the experimental one except that the maximum velocity appearing at the leading edge is overestimated. This is probably because a rapid increase in the horizontal velocity was not measured in the hydraulic model experiment due to the limitation of propeller current meter which is not suitable for highly fluctuating velocities.

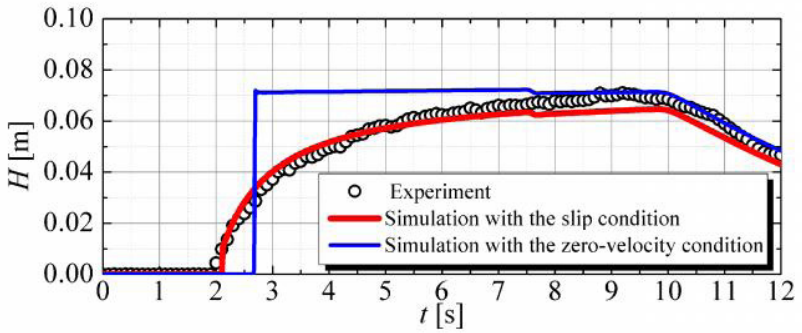

(a) Inundation depth

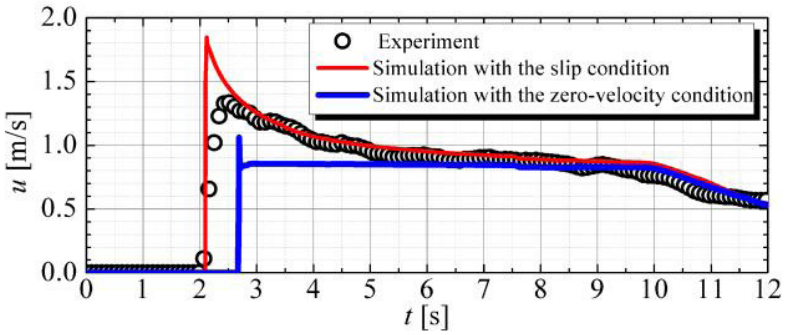

(b) Horizontal velocity

Figure 4. Comparison between numerical and experimental results at $x = -1.0$ m.

4.2. Effect of overflow condition

Considering the above results, this section discusses the effect of the overflow condition based on the numerical results employing the slip condition as the wet-dry condition.

Figures 5 and 6 show water surface profiles for the overflow conditions with and without the overflow formula, in which (a), (b) and (c) indicate the cases of H_w = 0.02 m, 0.05 m and 0.11m, respectively. It can be seen from these figures that free-surfaces have different profiles between the overflow conditions. In the condition with the overflow formula, the water level reaches a maximum near the seawall, and gradually decreases toward the wave front. On the other hand, there is little change in the water level near the seawall in the condition without the overflow formula.

Comparisons between numerical and experimental results for the time series of water depth and horizontal velocity at x = -1.0 m are shown in Figs. 7 and 8. There is no significant difference for the overflow conditions in terms of the tsunami arrival time. In the condition with the overflow formula shown in Fig. 7 (a), the numerical results are overestimated for all the seawall heights for $t > 4$ s although the numerical results are in a good agreement with the experimental ones for a period just after the bore passed. In the condition without the overflow formula indicated in Fig. 7 (b), there is a good agreement between the numerical and the experimental results for all periods except for the cases with the large height of the seawall (H_w =0.09 m and 0.11 m).

According to the experimental results for the horizontal velocity shown in Fig. 8, a reduction of the horizontal velocity due to the seawall is not significant under the conditions for the seawall heights of H_w = 0.02 m, 0.05 m and 0.07 m, and the horizontal velocity is confirmed to decrease with increasing the seawall height for the cases with the seawall heights $H_w > 0.09$ m. It can be seen from Fig. 8 (a) that the horizontal velocity simulated using the overflow formula shows different tendency with the experimental ones and the horizontal velocity is reduced with the increase of the seawall height even for the cases with the seawall height H_w = 0.02 m, 0.05 m and 0.07 m. As a result, the numerical results are underestimated except for the case with the seawall height of H_w = 0.11 m. In the condition without the overflow formula, the numerical results coincides with the experimental one for the cases with the seawall heights H_w = 0.02 m, 0.05 m and 0.07 m although the results are overestimated for the cases with large height of the seawall as well as the inundation depth. One of the reason is that the present model does not consider energy losses related to the overflow process.

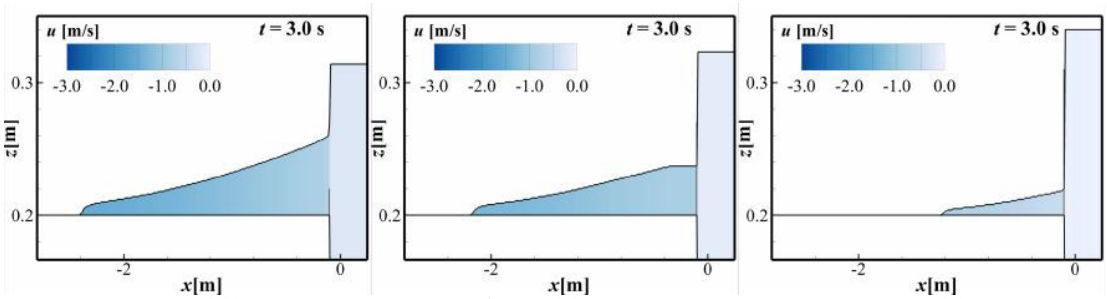

(a) H_w = 0.02 m (b) H_w = 0.07 m (c) H_w = 0.11 m

Figure 5. Water surface profile and horizontal velocity distributions for the condition with the overflow formula.

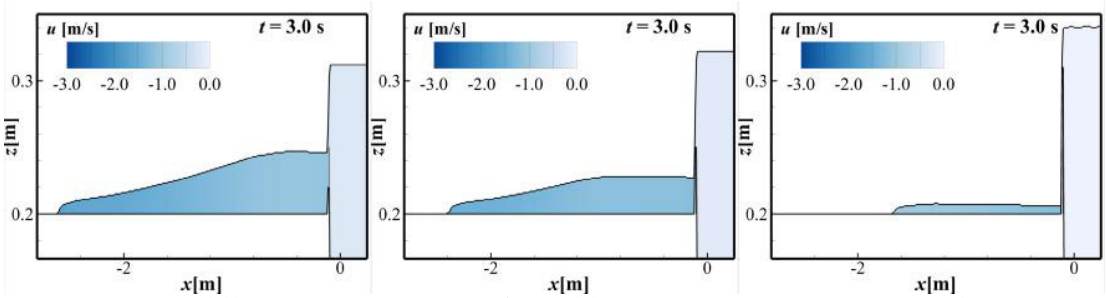

(a) H_w = 0.02 m (b) H_w = 0.07 m (c) H_w = 0.11 m

Figure 6. Water surface profile and horizontal velocity distributions for the condition without the overflow formula.

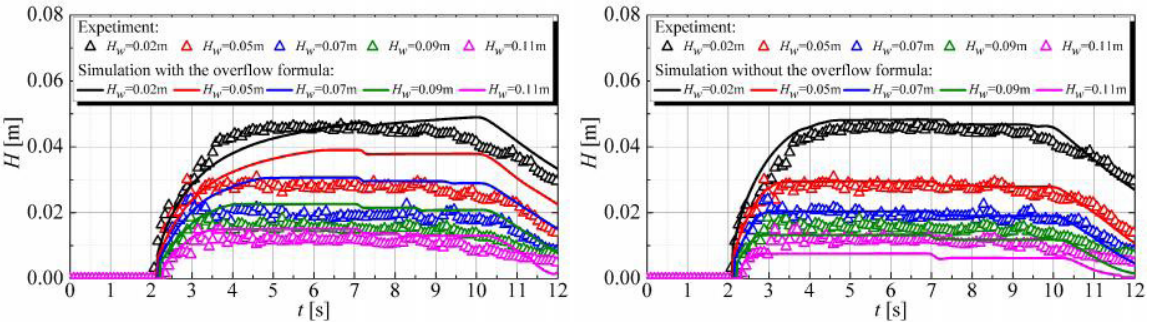

(a) With the overflow formula (b) Without the overflow formula

Figure 7. Comparison between numerical and experimental results of time series of water depth at x = -1.0 m

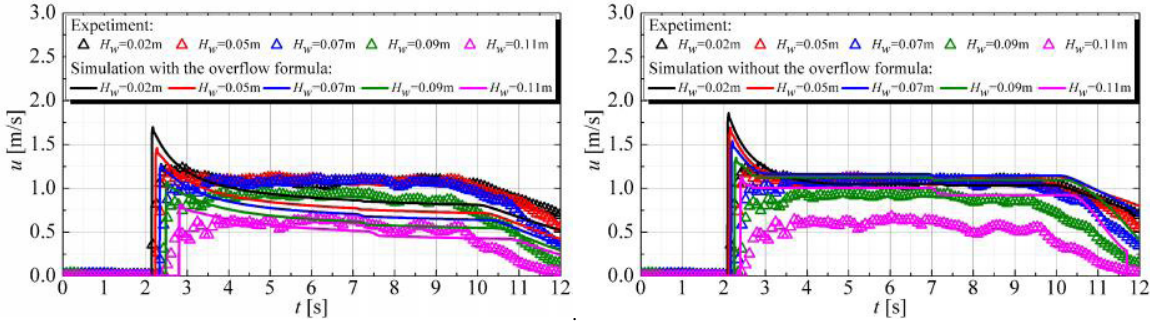

(a) With the overflow formula (b) Without the overflow formula

Figure 8. Comparison between numerical and experimental results of time series of horizontal velocity at x = -1.0 m.

5. Conclusion

This study has developed a two-dimensional tsunami run-up model using the CIP method, which is a high accuracy advection scheme, so as to satisfy the continuity equation with reasonable accuracy. Numerical simulations on tsunami bore have been carried out to validate the model and discussed the effects of wet-dry condition and overflow condition on the calculation accuracy. As a result, it was revealed that the model developed here is capable of representing closely actual water surface profile by using the slip condition on the wet-dry condition. Furthermore, the numerical results without the overflow formula were shown to be in good agreement with the experimental ones.

Acknowledgements

This research is supported in part by the Aid Project for the Strategic Research Foundation at Private Universities of the Ministry of Education, Culture, Sports, Science and Technology, Japan (No. S1201023, Head Investigator: T. Kodaka (Meijo University)).

References

Arimitsu, T., K. Ooe, and K. Kawasaki. 2013. Evaluation method of tsunami wave pressure acting on land structure using 2D depth-integrated flow simulation, Proceedings of 7th International Conference on Coastal Dynamics, ASCE, 466-480.

Honma, H., 1940. Flow Rate Coefficient of Low-overflow Dams, Journal of Civil Engineering, 26, 6, pp. 635-645 (in Japanese).

Kawasaki, K.. 2005. Numerical Model of 2-D Multiphase Flow with Solid-Liquid-Gas Interaction, International Journal of Offshore and Polar Engineering, 15, 3, pp. 198-203.

Kawasaki, K., T. Ono, N. Piamsa-nga, H. Atsuta, and K. Nakatsuji, 2004. Development of depth-averaged inundation flow model based on CIP method and SMAC method, Proceedings of Hydraulic Engineering, JSCE, 48, 565-570 (in Japanese).

Kotani, M., F. Imamura, and N. Shuto. 1998. Tsunami run-up simulation and damage estimation by using GIS, Proceedings of Coastal Engineering, JSCE, 45, pp. 356-360 (in Japanese).

Liang, Q., and F. Marche. 2009. Numerical resolution of well-balanced shallow water equations with complex source terms, Advances in water resources, 32, 6, pp.873-884.

Yabe, T. and T. Aoki. 1991. A universal solver for hyperbolic equations by cubic-polynomial interpolation I. One-dimensional solver. Computer Physics Communications, 66, 2, 219-232.

Yabe, T., F. Xiao and T. Utsumi. 2001. The Constrained Interpolation Profile Method for Multiphase Analysis, Journal of Computational Physics, 169, 2, pp.556-593.

Yoon, T. H. and S. K. Kang. 2004. Finite volume model for two-dimensional shallow water flows on unstructured grids, Journal of Hydraulic Engineering, 130, 7, pp.678-688.